Parallel MRI Reconstruction Using Variance Partitioning Regularization

Fa-Hsuan Lin,[1,2]* Fu-Nien Wang,[3] Seppo P. Ahlfors,[1,2] Matti S. Hämäläinen,[1,2] and John W. Belliveau[1,2]

Multiple receivers can be utilized to enhance the spatiotemporal resolution of MRI by employing the parallel imaging technique. Previously, we have reported the L-curve Tikhonov regularization technique to mitigate noise amplification resulting from the geometrical correlations between channels in a coil array. Nevertheless, one major disadvantage of regularized image reconstruction is lengthy computational time in regularization parameter estimation. At a fixed noise level, L-curve regularization parameter estimation was also found not to be robust across repetitive measurements, particularly for low signal-to-noise ratio (SNR) acquisitions. Here we report a computationally efficient and robust method to estimate the regularization parameter by partitioning the variance of the noise-whitened encoding matrix based on the estimated SNR of the aliased pixel set in parallel MRI data. The proposed Variance Partitioning Regularization (VPR) method can improve computational efficiency by 2–5-fold, depending on image matrix sizes and acceleration rates. Our anatomical and functional MRI results show that the VPR method can be applied to both static and dynamic MRI experiments to suppress noise amplification in parallel MRI reconstructions for improved image quality. Magn Reson Med 58:735–744, 2007. © 2007 Wiley-Liss, Inc.

Key words: regularization; VPR; SNR; L-curve; SVD; variance partitioning; Tikhonov; parallel MRI; SENSE

The recent development of parallel MRI acquisition can enhance the spatiotemporal resolution of MRI in both anatomical and functional scans. Parallel MRI utilizes an RF coil array to simultaneously acquire data from multiple receivers, and acceleration is achieved by a reduced phase-encoding *k*-space trajectory. The nature of the subsampled *k*-space trajectory requires the use of a reconstruction algorithm to restore aliased images into full field-of-view (FOV) images. Previously proposed reconstruction algorithms include the *k*-space-based SMASH method (1) and the image domain-based SENSE approach (2). In addition to improving the spatiotemporal resolution, parallel MRI can reduce the image distortion in echo-planar imaging (EPI) (3) or diminish the acoustic noise by lowering gradient switching rates (4). Nevertheless, these advantages come at the cost of lowered signal-to-noise ratio (SNR) because the number of acquired data samples in parallel MRI is reduced. In addition, reconstructing parallel MRI acquisitions heavily depends on the independent information from each channel in an RF coil array. Correlations in spatial information caused by the geometric arrangement of the array element can deteriorate image quality. To mitigate this issue, researchers have previously optimized coil geometry (5) or improved the stability of the reconstruction algorithm. The increased noise originating from correlated spatial information in the array elements can be estimated based on the array geometry and quantified by a geometric factor (g-factor) (2).

Previously, we proposed to minimize the g-factor by using a full-FOV reference scan to provide prior information and to stabilize image reconstruction. The method was based on the Tikhonov regularization framework (6) to reduce the noise amplification of parallel MRI reconstruction when the encoding matrix is ill-conditioned. Applying regularized SENSE imaging to anatomical and dynamic functional MRI of human brain reduced the noise level and enabled higher detection power in acquisitions with high acceleration rates (7,8). The importance of choosing appropriate regularization parameters has also been reported for different parallel MRI reconstruction algorithms with versatility in the choice of prior information and a regularization parameter (9–13). However, one disadvantage of regularized parallel MRI reconstruction is the computational time associated with regularization parameter estimation. In order to estimate a regularization parameter, the L-curve approach requires an iterative search for each set of aliased image pixels; each iteration step involves calculations of prior error and model error terms (7). As clearly demonstrated in this study, another challenge of the L-curve method is instability. Given a fixed noise level, the regularization parameter estimated by L-curve may vary significantly, potentially due to an ill-defined "elbow" region in L-curve calculation. This problem is particularly more prominent in low SNR acquisitions, where regularization is more crucial for suppressing noise in reconstruction.

The purpose of this study is to propose an alternative method to calculate a regularization parameter in parallel MRI reconstruction with improved computational efficiency and reduced variability in regularization parameter estimation. In this article we present a fast and robust method to estimate regularization parameters without an iterative search. The SNR of the set of aliased pixels in

[1]Institute of Biomedical Engineering, National Taiwan University, Taipei, Taiwan.

[2]MGH-HMS-MIT Athinoula A. Martinos Center for Biomedical Imaging, Massachusetts General Hospital, Charlestown, Massachusetts.

[3]Department of Biomedical Engineering and Environmental Sciences, National Tsing Hua University.

Grant sponsor: National Institutes of Health (NIH); Grant numbers: R01 HD040712, R01 NS037462, R01 EB000790, P41 RR14075; Grant sponsor: Mental Illness and Neuroscience Discovery Institute (MIND).

Part of this work has been presented in the 2nd International workshop on parallel MRI, Zurich, Switzerland in October, 2004

*Correspondence to: Fa-Hsuan Lin, PhD, Athinoula A. Martinos Center for Biomedical Imaging, Bldg. 149 13th St., Mailcode 149-2301, Charlestown, MA 02129. E-mail: fhlin@nmr.mgh.harvard.edu; Institute of Biomedical Engineering, National Taiwan University, 1, Sec. 4, Roosevelt Rd., Taipei, 106, Taiwan.

Received 24 August 2006; revised 1 February 2007; accepted 13 June 2007.

DOI 10.1002/mrm.21356

Published online in Wiley InterScience (www.interscience.wiley.com).

parallel MRI data is estimated and used to partition the singular value spectrum of the encoding matrix for regularization parameter estimation. Unlike other implementations of regularization parameter estimation algorithms that utilize minimal heuristic intervention (12,13), the Variance Partitioning Regularization (VPR) method introduced here is fully automatic and adapts to the noise level of the acquired data. We evaluated the performance of VPR in terms of the variability of the estimated regularization parameter, the quality of the reconstructed image, and computational time using anatomical and functional MRI data.

THEORY

The process of generating a parallel MRI dataset can be formulated as a linear operation to "fold" the full-FOV spin density image:

$$\bar{\mathbf{y}} = \mathbf{A}\bar{\mathbf{x}} + \bar{\mathbf{n}} \qquad [1]$$

Here $\bar{\mathbf{y}}$ is a vertically stacked vector consisting of aliased images on each channel in the array, $\bar{\mathbf{n}}$ is the contaminating noise in the array channels, and $\bar{\mathbf{x}}$ is the vector representing the full-FOV image to be reconstructed. The encoding matrix $\mathbf{A}$ consists of the product of the aliasing operation due to subsampling of the *k*-space data and coil-specific spatial sensitivity modulation over the FOV. The goal of parallel MRI image reconstruction is to solve for $\bar{\mathbf{x}}$ given our knowledge of $\mathbf{A}$ derived from the *k*-space trajectory and estimates of the coil sensitivity maps. Note that Eq. [1] is valid for both image domain-based SENSE (2) and *k*-space-based SMASH (1,14) methods. Without loss of generalization, we focus this article on SENSE imaging reconstruction. In general terms, Eq. [1] is an overdetermined linear system; i.e., the number of array coils n_c, the dimension of $\tilde{\mathbf{y}}$, exceeds the number of the pixels folding into a measured pixel, the dimension of $\tilde{\mathbf{x}}$.

Using Tikhonov regularization, unfolding aliased images from an array can be formulated as an optimization problem minimizing the following cost function (7):

$$\bar{\mathbf{x}}^{\lambda} = \arg\min_{\bar{x}}\{\|\tilde{\mathbf{A}}\bar{\mathbf{x}} - \tilde{\mathbf{y}}\|_2{}^2 + \lambda\|\mathbf{L}(\bar{\mathbf{x}} - \bar{\mathbf{x}}^0)\|_2{}^2\}, \qquad [2]$$

where λ is the regularization parameter, $\mathbf{L}$ is a positive semi-definite linear transformation, and $\tilde{\mathbf{x}}^{\mathbf{0}}$ denotes the prior information about the solution $\tilde{\mathbf{x}}$. Here $\|\cdot\|_2$ represents the ℓ_2-norm; $\tilde{\mathbf{A}}$ and $\tilde{\mathbf{y}}$, respectively, are the spatially whitened encoding matrix and observation vector (7).

$$\tilde{\mathbf{y}} = \mathbf{\Phi}^{-1/2}\bar{\mathbf{y}}$$
$$\tilde{\mathbf{A}} = \mathbf{\Phi}^{-1/2}\mathbf{A}, \qquad [3]$$

where $\mathbf{\Phi}^{-1/2}$ is the Cholesky decomposition of the noise covariance matrix $\mathbf{\Phi}$ among channels in an RF coil array.

Given a regularization parameter λ and letting $\mathbf{L}$ be an identity matrix, the solution of Eq. [2] has been derived by Hansen (15). To quantify the noise amplification introduced during SENSE reconstruction, we can use the geometrical factor (g-factor) as the ratio of the noise levels between the regularized parallel MRI reconstruction and the original full-FOV image, normalized by the acceleration rate (2). We have previously derived the g-factor for regularized reconstructions (7).

Estimation of Regularization Parameter by Variance Partitioning Regularization (VPR)

Here we propose to estimate the regularization parameter by partitioning the singular value spectrum of the noise whitened encoding matrix into "signal" and "noise" parts in order to match the estimated SNR of the measurements. Qualitatively, when the encoding matrix consists of noisy transformation, more dependency on the prior information of the solution (and thus a larger regularization parameter) can improve the robustness of the solution. This corresponds to partitioning the encoding matrix into few dominant singular values/vectors in the "signal" part and the majority of others in the "noise" part. On the contrary, if the encoding matrix consists of stable and low noise transformation, credible RF array observations can be used directly to solve for the spin density distribution without being biased toward prior information. This corresponds to a scenario with a small regularization parameter and the majority of singular values/vectors in the encoding matrix are partitioned into the "signal" part. In summary, the decomposition of the encoding matrix can thus be coupled to the SNR of the measurement in regularization parameter estimation.

To implement this concept, we must first estimate a scalar SNR of the aliased pixel set from all channels in the RF coil array before estimating a scalar regularization parameter. In fact, the whitening procedure in Eq. [3] transformed the measurements from all channels of the array from signal amplitude into noise-normalized signal amplitude, since the data from all channels were divided by a pre-whitening matrix, which is essentially the estimated noise level in a matrix formulation. After whitening, data from all channels of the array were in an SNR-like unit. Thus, the maximum across whitened measurements can be considered the "peak" SNR, and the average across them can be considered the "averaged" SNR. We propose to estimate a scalar peak SNR (pSNR) across channels in the array from whitened observations as:

$$\mathrm{pSNR} \approx \max\{diag(\tilde{\mathbf{y}}\tilde{\mathbf{y}}^H)\} - 1. \qquad [4]$$

Here $diag(\cdot)$ refers to taking diagonal entries from a matrix. And $\max\{\cdot\}$ refers to searching for the maximal value from the input vector.

Alternatively, we may provide an estimate of average SNR (aSNR) across channels in the array from whitened observations as:

$$\mathrm{aSNR} \approx (\tilde{\mathbf{y}}^H\tilde{\mathbf{y}})/n_c - 1, \qquad [5]$$

where n_c is the number of channels in the array.

Given either pSNR or aSNR, we estimate the regularization parameter from the power spectrum of the singular values $\mathbf{S}_{ii}$ of the whitened encoding matrix $\tilde{\mathbf{A}}$ by searching

the singular value with index k such that the following cost function is minimized:

$$\lambda_{\mathrm{pSNR}} = \arg\min_{S_{kA}} \left(\left\| \mathrm{pSNR} - \left(\sum_{i=1}^{k} S_{ii}^2 \right) \Big/ \left(\sum_{i=k+1}^{n_c} S_{ii}^2 \right) \right\|_2^2 \right) \quad [6]$$

$$\lambda_{\mathrm{aSNR}} = \arg\min_{S_{kk}} \left(\left\| \mathrm{aSNR} - \left(\sum_{i=1}^{k} S_{ii}^2 \right) \Big/ \left(\sum_{i=k+1}^{n_c} S_{ii}^2 \right) \right\|_2^2 \right).$$

We term the methods giving λ_{pSNR} and λ_{aSNR} as pSNR-VPR and aSNR-VPR, respectively. Note that the regularization parameter here is estimated directly without iterative calculation, the most time-consuming process in the L-curve approach. Since aSNR $\leq$ pSNR, $\lambda_{\mathrm{pSNR}} \leq \lambda_{\mathrm{aSNR}}$. The partitioning of singular value variance is illustrated in Fig. 1.

MATERIALS AND METHODS

Static Anatomical Image Experiment

We attempted to evaluate the computational efficiency and the variability of the regularization estimates by the VPR algorithm and to compare it to the L-curve algorithm.

Using Monte Carlo simulations for VPR reconstructions, we used an 8-channel head coil array configuration consisting of 8 circular RF coils of 10 cm diameter. We positioned the individual circular RF coil circumferentially and equidistantly to cover a square FOV of 220 mm. We calculated the B_1 field maps of individual RF coils in the array based on the Biot-Savart's law that assumes a unit of current on each coil. In each channel of the array we multiplied a transverse slice anatomical image pixel-by-pixel by the simulated B_1 field to simulate the "signal" of an acquisition. The anatomical image was acquired from a 3T scanner (Siemens Medical Solutions, Erlangen, Germany) equipped with an 8-channel linear phased array coil that wraps around the head circumferentially. After obtaining approval from the Massachusetts General Hospital Institutional Review Board and informed consent, we used a 3D MPRAGE sequence to scan healthy subjects. The MPRAGE sequence parameters were TR = 500 ms, TE = 3.9 ms, flip angle = 20°, slice thickness = 1.33 mm, 48 slices, FOV = 210 × 210 mm, and image matrix = 256 × 256. Assuming minimal correlation among the channels in the RF array, we synthetically created acquisition "noise" for each channel by using a spatially uniform and uncorrelated Gaussian random noise model. In order to match to the SNR described in the derivation of VPR, the noise was linearly scaled such that the ratio between the top 1% of the power of simulated "signal" and the power of simulated "noise" equaled the specified SNR. Note that here SNR denoted power SNR rather than amplitude SNR. The simulated power SNRs varied between 100, 1000, and 10,000 (amplitude SNR of 10, 32, and 100, respectively). Each simulated acquisition was created for the 128 × 128 image matrix. At each simulation we used the pSNR-VPR and the L-curve methods to repeatedly calculate the regularization parameter at each frequency-encoding step with acceleration rates (R) of 2, 3, and 4 for 20 iterations, respectively. Additionally, we also calculated the regularization parameter using aSNR-VPR in each simulated power SNR in order to compare the reconstructions between aSNR-VPR and pSNR-VPR. To assess the computational efficiency of the regularization parameter estimation at different image matrix sizes, we resized the simulated data into 256 × 256, 128 × 128, and 64 × 64 image matrices. To quantify the reconstructions we calculated the variance of the residual image between the reconstruction and the original fully sample data in order to evaluate the severity of the image artifact.

In anatomical scans, practically we do not have prior information of the identical spatial resolution to the final reconstructed image. Thus, we also calculated the reconstruction regularized to a lower spatial resolution prior, which can be acquired from only a fraction of the central part of the k-space. For the reconstructed image matrix of 128 × 128, we parametrically changed the prior spatial resolution as 4 × 4, 8 × 8, 16 × 16, 32 × 32, and 64 × 64, respectively, in the 4-fold accelerated reconstructions using pSNR-VPR to study the effect of low spatial resolution prior.

The coil sensitivity maps required for SENSE reconstruction were estimated from a fully sampled dataset with a local polynomial fitting algorithm (2). All image reconstruction and regularization parameter estimations were performed on a Linux system with Pentium 4 2GB dual processors and codes written in MATLAB (MathWorks, Natick, MA).

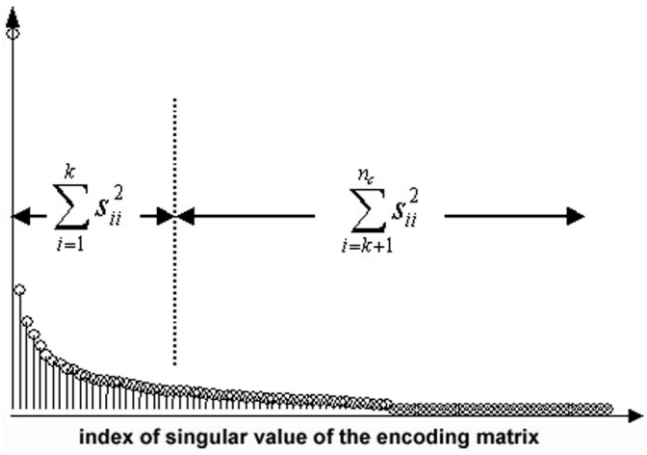

FIG. 1. Partitioning of the singular value spectrum of the encoding matrix to estimate the regularization parameter based on the SNR of the aliased pixels.

Dynamic fMRI Experiment

The fMRI experiment used the same 3T scanner and 8-channel head array as the anatomical experiment described above. With the approval from the MGH Institutional Review Board and informed consent we acquired echo-planar images (EPI) from healthy subjects. For simulations, baseline EPI images were collected with a 2D gradient echo EPI sequence (TR = 2000 ms, TE = 50 ms, flip angle = 90°, slice thickness = 5 mm with 0.5 mm gap, 14 slices, FOV = 192 mm × 192 mm, and image matrix = 64 × 64). The amplitude SNR of the EPI image was calculated from the root-sum-of-squares of EPI images combined from all channels of the RF array by the ratio be-

tween image intensity and background standard deviation. In the simulations we synthetically created time series of 100 images (8). Using zero-mean Gaussian noise, we adjusted the variance (estimated across timepoints) for all voxels such that the spatial distribution of amplitude SNR of all voxels matched the spatial distribution of the estimated amplitude SNR in baseline EPI measurements. The fMRI simulations generated different realizations of the noise at each timepoint. Each simulated fMRI time series consisted of 50 baseline images and 50 active images. BOLD contrast was first simulated at a spatially clustered region-of-interest (ROI) in the right hemisphere visual cortex (8-pixel-by-8-pixel, 576 mm^2). Here we varied two parameters in our numerical simulations: first, we changed BOLD contrasts parametrically from 1%, 2%, and 5–10%; second, we changed the SENSE acceleration rates from 2-fold and 3-fold to 4-fold. Both regularized and unregularized SENSE reconstructions were calculated to restore the unaliased full-FOV fMRI time series.

To validate and to compare VPR reconstructions in fMRI, we used the "fractional principle singular value (fPSV)" method to estimate the regularization parameters. The fPSV approach used a fixed fraction (1/20) of the first singular value of the encoding matrix as the regularization parameter (14). Reconstructions of unregularized, fPSV regularized, aSNR-VPR, and pSNR-VPR were all calculated.

For in vivo fMRI experiments we used a 4-Hz checkerboard visual stimulus presented by E-PRIME (Psychology Software Tools, Pittsburgh, PA). The visual stimulus was designed to display either continuous flashing checkerboards at 4 Hz for 30 sec (the "on" condition), or fixation cross only for 30 sec (the "off" condition). Four "off" and three "on" conditions were alternatively presented to each subject, starting with the "off" condition. Image acquisition used a 2D gradient echo EPI sequence with parameters of TR = 1500 ms, TE = 30 ms, flip angle = 90°, slice thickness = 5 mm with 1 mm gap, 24 slices, FOV = 200 × 200 mm, and image matrix = 64 × 64. We employed interleaved 4-segment EPI to obtain 4-fold acceleration.

Both the simulations and fMRI experimental data were reconstructed by the "in vivo sensitivity" SENSE reconstruction method (14), which estimates the dynamic change of the ratio of the spin density in each SENSE-reconstructed scan over that in a reference scan with full phase-encoding. The reference scans were derived from combining interleaved EPI segments (8). To compare reconstruction results, we calculated SENSE reconstructions of each image using L-curve regularization and aSNR-VPR. We used the AFNI software package (http://afni.nimh.nih.gov/) (25) for subsequent motion correction of interscan head motion by registering each reconstructed EPI volume to the mean of its time series with a linear 6-parameter rigid-body transformation model. We applied a 3D Gaussian filter (full-width-half-maximum, FWHM, of 6 mm in all dimensions) to each volume in the time series for spatial smoothing. Finally, we performed a *t*-test (26) on the reconstructed SENSE fMRI to contrast the "on" and the "off" conditions.

RESULTS

Variability of Regularization Parameters

Figure 2 shows one realization of the sum-of-square combined images from all channels in the RF array and one representative RF coil image around the temporal lobe at power SNRs of 100, 1000, and 10,000. The variability of estimated regularization parameters using pSNR-VPR, aSNR-VPR, and L-curve algorithms at different simulated power SNRs across frequency-encoding steps is shown in Fig. 3. Note that in general the pSNR-VPR method provided smaller regularization parameters than the L-curve method. Among realizations of the simulated data in each power SNR, the variability of regularization parameters estimated by the L-curve method was much greater than that by the pSNR-VPR method. Note that aSNR-VPR estimated similar regularization parameter to the L-curve results at high acceleration rates (>3× acceleration) and low-power SNR (power SNR = 100). At higher power SNR and smaller acceleration rate, pSNR-VPR and aSNR-VPR results were similar. We found that at either end of the frequency-encoding steps L-curve and VPRs reported larger variability on the estimated regularization parameters, potentially due to low-intensity air regions in the image and associated low SNR in these areas. Table 1 reports the median of the ratios between the mean and the standard deviation of the estimated regularization parameters across simulations using L-curve and pSNR-VPR methods at different power SNRs. We chose to report median rather than mean values in order to provide more robust

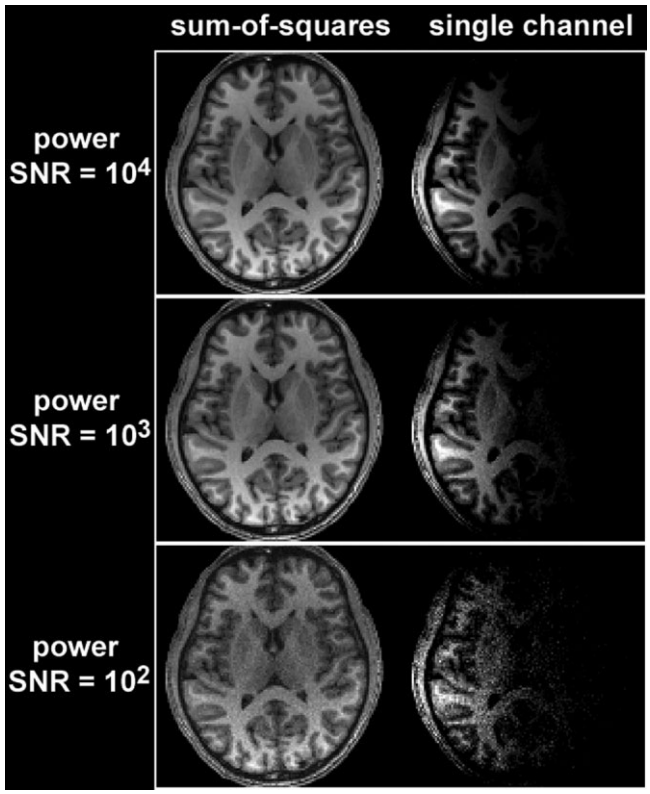

FIG. 2. One realization of the sum-of-square combined image and the single channel RF coil image around the temporal lobe at power SNR = 100, 1000, and 10,000.

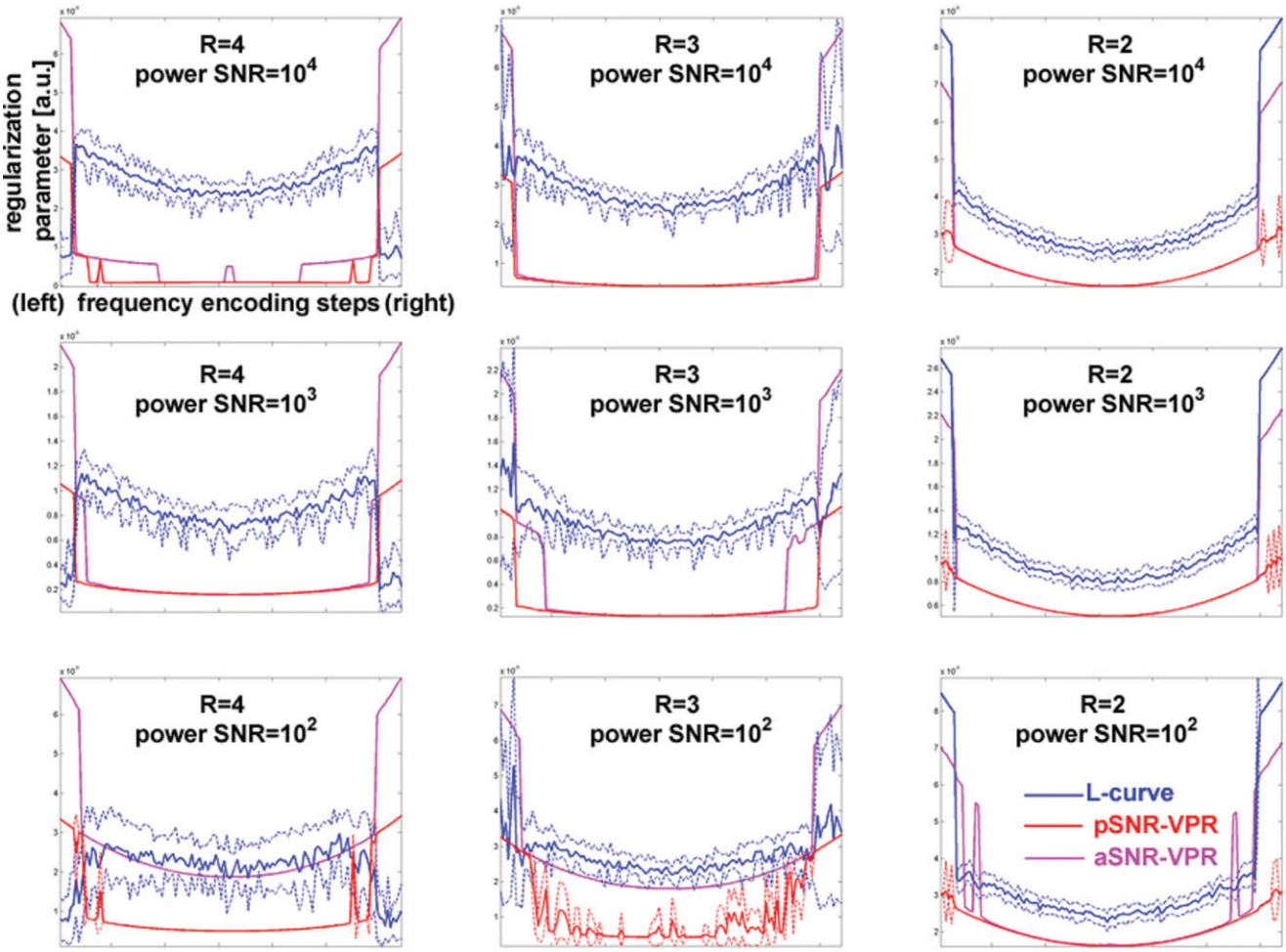

FIG. 3. Regularization parameters at different frequency-encoding steps using L-curve regularization (blue trace), pSNR-VPR (red trace), and aSNR-VPR (pink trace) at 2-fold, 3-fold, and 4-fold SENSE accelerations. The solid lines are the averaged regularization parameters in 20 repetitive simulations. The dashed lines show the estimated regularization parameters with +1 and −1 standard deviation on top of the average in 20 repetitive simulations.

assessment of the variability around the center of the FOV, without being biased from the high variability around either end of the frequency steps. Compared to L-curve, pSNR-VPR significantly reduced the variability of the regularization parameter from between 7% and ≈30% to 1% or less. On average, pSNR-VPR was associated with 10-fold or greater improvement in the variability of estimated regularization parameters.

Computational Efficiency

Table 2 lists the times required to estimate regularization parameters at different image matrix sizes and SENSE acceleration rates. Note that the time required for regularization parameter estimation grows nonlinearly with image matrix size, independent of the regularization parameter estimation approach used. The combination of larger image matrix and smaller acceleration rate requires more time to estimate the regularization parameter because the number of aliased pixel sets is larger. At higher acceleration rate, we found that less time was required for regularization parameter estimation, potentially because fewer data samples were used in the calculation. When image matrix size and SENSE acceleration rate were equal, pSNR-VPR took less time than the L-curve approach. The computational time saved for regularization parameter estimation by the pSNR-VPR approach may be as high as 2–5-fold, depending on the image matrix size and

Table 1
Variability of the Estimated Regularization Parameter Using L-curve or pSNR-VPR

Power SNR	R	L-curve	pSNR-VPR
10,000	2	7.35%	0.19%
	3	8.86%	0.22%
	4	10.84%	0.17%
1000	2	7.47%	0.17%
	3	16.71%	0.20%
	4	17.76%	0.21%
100	2	8.25%	0.19%
	3	16.84%	1.77%
	4	33.63%	0.26%

Here variability was defined as the ratio of the standard deviation over the mean of estimated regularization parameter. To avoid the bias from high variability around air regions in the image, we reported the median of the ratios across frequency-encoding steps.

Table 2
Computational Time for Regularization Estimation Using Either pSNR-VPR or L-curve Approach for 256 × 256, 128 × 128, and 64 × 64 Image Matrix at 2.0-fold, 3.0-fold, and 4.0-fold SENSE Accelerations

SENSE acceleration	Image matrix	pSNR-VPR (sec)	L-curve (sec)	Computational time with respect to L-curve
2.0	64 × 64	0.94	5.04	19%
	128 × 128	13.75	31.06	44%
	256 × 256	353.70	594.63	59%
3.0	64 × 64	0.72	2.65	27%
	128 × 128	11.17	23.07	48%
	256 × 256	342.08	614.86	56%
4.0	64 × 64	0.67	2.51	27%
	128 × 128	10.55	21.06	50%
	256 × 256	275.70	405.57	68%

The computational efficiency of pSNR-VPR and aSNR-VPR are identical.

SENSE acceleration rates. Significant improvement in computational efficiency was observed in cases of small matrix size (64 × 64 image matrixes). Since aSNR-VPR and pSNR-VPR only differ at the partitioning point in the singular value spectrum of the whitened encoding matrix, the computational efficiency of both VPR alternatives is identical.

Anatomical MRI

Figure 4 shows the SENSE-reconstructed images using either no regularization or regularization parameters estimated by the L-curve, pSNR-VPR, and aSNR-VPR methods. At 2-fold acceleration, all reconstructions (unregularized, L-curve, and VPRs) yielded satisfactory reconstructions at high-power SNR (power SNR ≥1000). At lower power SNR (power SNR = 100), unregularized reconstruction showed noisy reconstruction at the center of the FOV. At 3-fold acceleration, unregularized reconstructions were noisy at power SNRs of 100 and 1000. Compared to the unregularized reconstructions, either L-curve or VPR reconstructions showed improved image quality. Note that because smaller regularization parameters were employed, pSNR-VPR reconstructions were noisier than L-curve reconstructions. However, using aSNR-VPR, the reconstruction is similar to that using the L-curve regularization, particularly at low-power SNR simulations at high (3-fold) acceleration rate. At 4-fold acceleration, unregularized results were too noisy to discern anatomical structures; however, reconstructions regularized by L-curve, aSNR-VPR, and pSNR-VPR did show anatomical structures. Again, aSNR-VPR used a higher regularization to suppress more noise than pSNR-VPR and thus the reconstruction was of higher quality. The variances of the residual images between the reconstructions and the fully sampled image are also reported in Fig. 4. These error metrics quantitatively validated the improved reconstruction of aSNR-VPR described above. Figure 5 shows the regularized reconstructions at lower SNR (power SNR = 100) and high (4-fold) acceleration. We found that the L-curve reconstruction showed variable reconstruction quality across frequency-encoding steps. This is due to the nonsmooth estimated

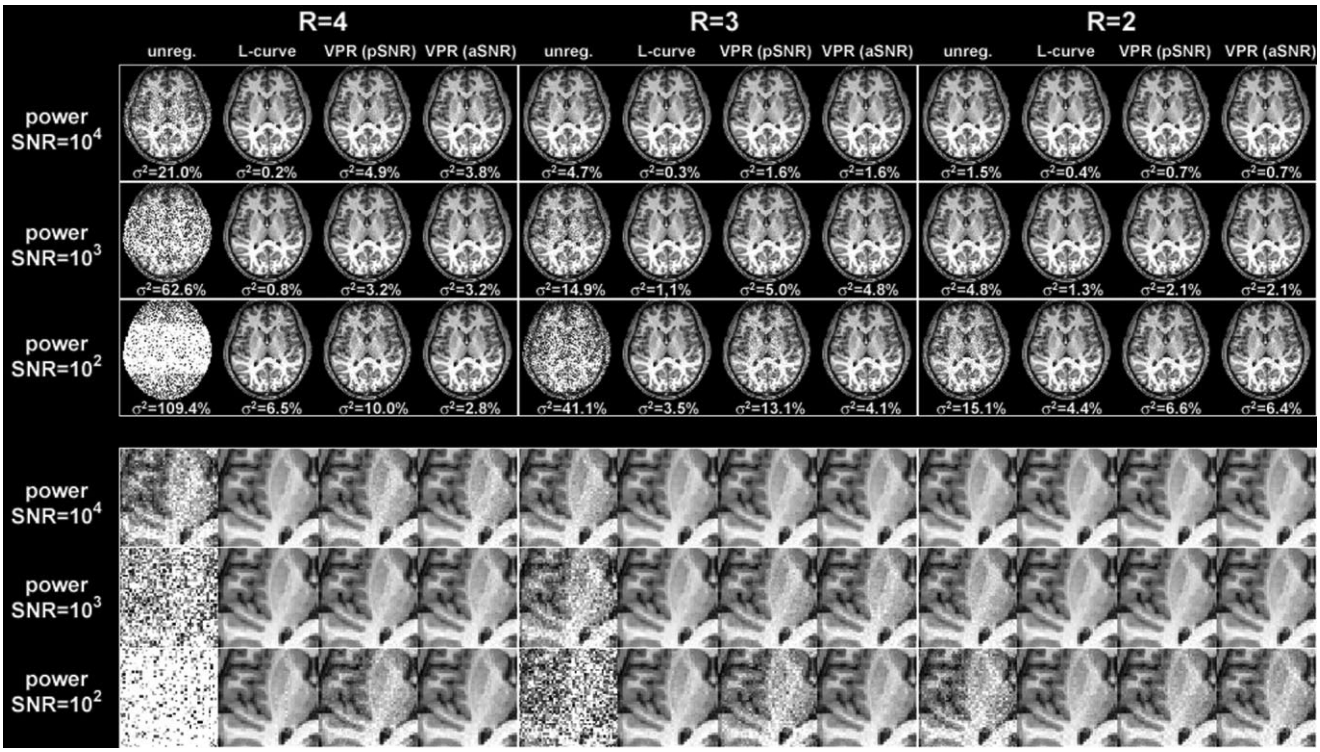

FIG. 4. (top) The reconstructed SENSE images using L-curve regularization, pSNR-VPR, and aSNR-VPR at 2-fold, 3-fold, and 4-fold SENSE accelerations. (bottom) The same reconstructed image magnified around the temporal lobe. The variance (σ^2) of the residual image between a reconstruction and the fully sampled image was also reported.

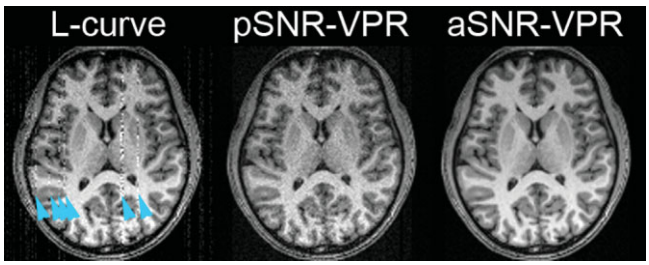

FIG. 5. Details of the L-curve, pSNR-VPR, and aSNR-VPR reconstructions at power SNR = 100 and 4-fold acceleration. The noticeable discontinuity across frequency-encoding steps in the L-curve reconstruction is marked with arrowheads.

regularization parameter shown in Fig. 3. pSNR-VPR reconstruction was continuous across frequency-encoding steps, but the overall image quality is more noisy due to low regularization parameters. aSNR-VPR reconstruction showed smooth and low-noise reconstruction due to a higher regularization than pSNR-VPR.

The results of pSNR-VPR reconstructions using low-resolution priors are shown in Fig. 6. We observed that for 4-fold accelerated data with high SNR (power SNR = 10^4), even prior with 1/8 spatial resolution of the final reconstructed image can make basal ganglia distinguishable compared to the noisy unregularized reconstruction. Priors with 1/4 spatial resolution of the final reconstructed image made dramatic improved reconstructions in low, intermediate, and high SNRs (power SNR = 10^2, 10^3, and 10^4, respectively). The error metrics are also shown in Fig. 6, corresponding to a monotonically decrease of the reconstruction error as either power SNR or prior spatial resolution increases. We noticed that providing low-resolution prior led to reconstructions with noticeable aliasing artifacts. This is because the prior did not contain high *k*-space data, and therefore biasing toward the low-resolution prior caused suppressed the reconstructions at the skipped *k*-space lines during the accelerated scans.

Functional MRI

In dynamic imaging, dependency on prior information can reduce image contrast, while regularization can reduce noise level. Here we investigated the overall consequence of contrast-to-noise ratio (CNR) of regularized reconstructions in dynamic fMRI experiments. Figure 7 shows simulations of *t*-statistics maps using SENSE acquisition and regularized reconstructions overlaid on a fully sampled EPI data. Note that all SENSE reconstructions at 2-fold and 3-fold accelerations were able to detect the implanted active region. We found that regularized reconstructions by aSNR-VPR, pSNR-VPR, or fPSV outperformed the unregularized reconstructions. Furthermore, both aSNR-VPR and pSNR-VPR regularized reconstruction had improved detection sensitivity compared to fPSV. At 4-fold acceleration the detection power of the unregularized reconstruction dropped significantly. On the contrary, pSNR-VPR, aSNR-VPR, and fPSV regularized reconstruction can maintain detection at 4-fold acceleration and showed reduced false-negative detection. The increased detection power of regularized SENSE reconstruction using either the fPSV or the pSNR-VPR method was observed in BOLD contrasts ranging between 1% and 10%. One reason to account for these findings is that the suppression of the noise superseded the suppression of dynamic contrast in regularization, leading to a final improved CNR quantified by the *t*-statistics. This matched our previous study using the L-curve regularization to provide improved fMRI sensitivity (8). Even though showing improved detection compared to the unregularized reconstructions, the fPSV method did not provide the optimal regularization parameter to maximize the *t*-statistics. Both aSNR-VPR and pSNR-VPR are data-driven approaches. Thus, they are both adaptive to the quality of the acquisitions and the resultant regularized reconstructions showed even more improved detection power compared to fPSV.

Figure 8 shows the *t*-statistics maps of the in vivo visual fMRI experiment overlaid on the EPI-averaged images. Six slices covering the occipital lobe visual cortex activations for four subjects are shown at 4-fold SENSE accelerations using L-curve, aSNR-VPR, and fPSV reconstructions. Statistically significant functional activations in the visual cortex were detected for all subjects. Comparable sizes of functional areas were identified by L-curve and aSNR-VPR reconstructions. fPSV reconstructions show reduced functional activation.

DISCUSSION

In this article we propose a computationally efficient and robust approach for regularization parameter estimation. Previously, it has been shown that regularized SENSE imaging reconstruction can reduce noise amplification attributable to an ill-posed encoding matrix (7). Such singularity primarily derives from the geometrical arrangement of the array coil and reduced data acquisition, and it leads to significant uncertainty about the estimated spin density. Recently, we showed that regularized SENSE reconstruction is helpful for improving the detection power of the fMRI experiment, particularly when SENSE acceleration rate is high (8). Regularization is thus desired to improve SENSE reconstruc-

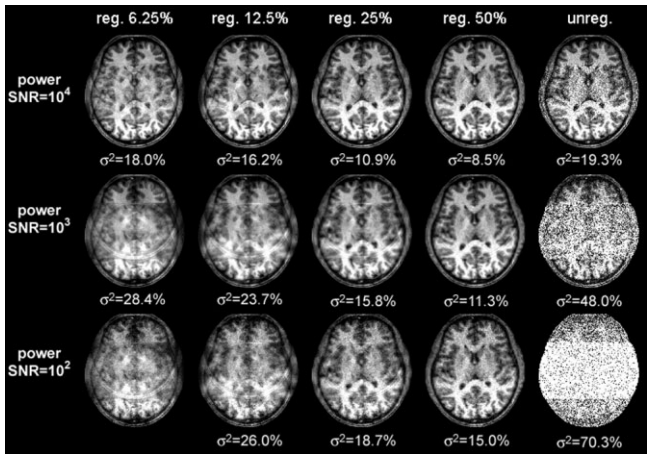

FIG. 6. Four-fold unregularized and pSNR-VPR reconstructions using different low-resolution priors at different SNRs. The variance (σ^2) of the residual image between a reconstruction and the fully sampled image is also reported.

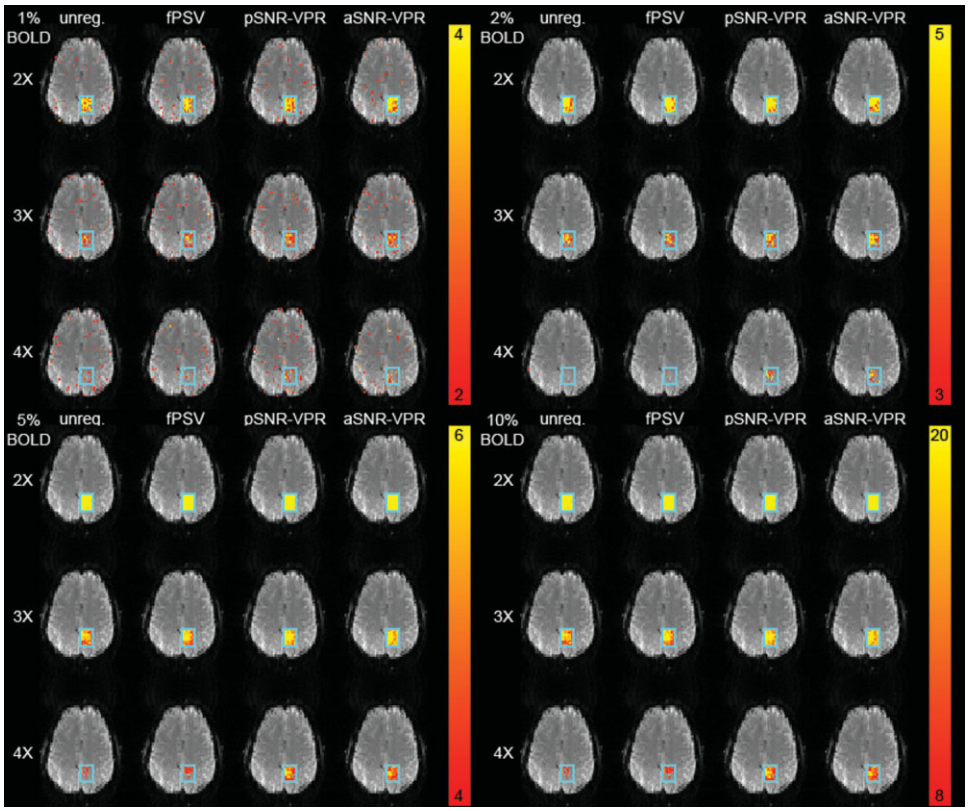

FIG. 7. The *t*-statistics maps from the simulation using 2-, 3-, and 4-fold SENSE accelerations without regularization or with fPSV regularization, pSNR-VPR, and aSNR-VPR. The light blue box at the right occipital lobe indicates the region of synthetic BOLD contrast.

tions of high acceleration SENSE imaging for structural and functional dynamic MRI experiments.

In this study, through simulations we found that the regularization parameter estimated by the L-curve method showed higher variability across frequency-encoding steps in simulations. The reason to use simulations is that the L-curve is not a linear method and currently there exists no analytical solution about its stability and sensitivity to noises. Additionally, the L-curve approach is data-dependent, since it needs to calculate not only the prior error term but also the

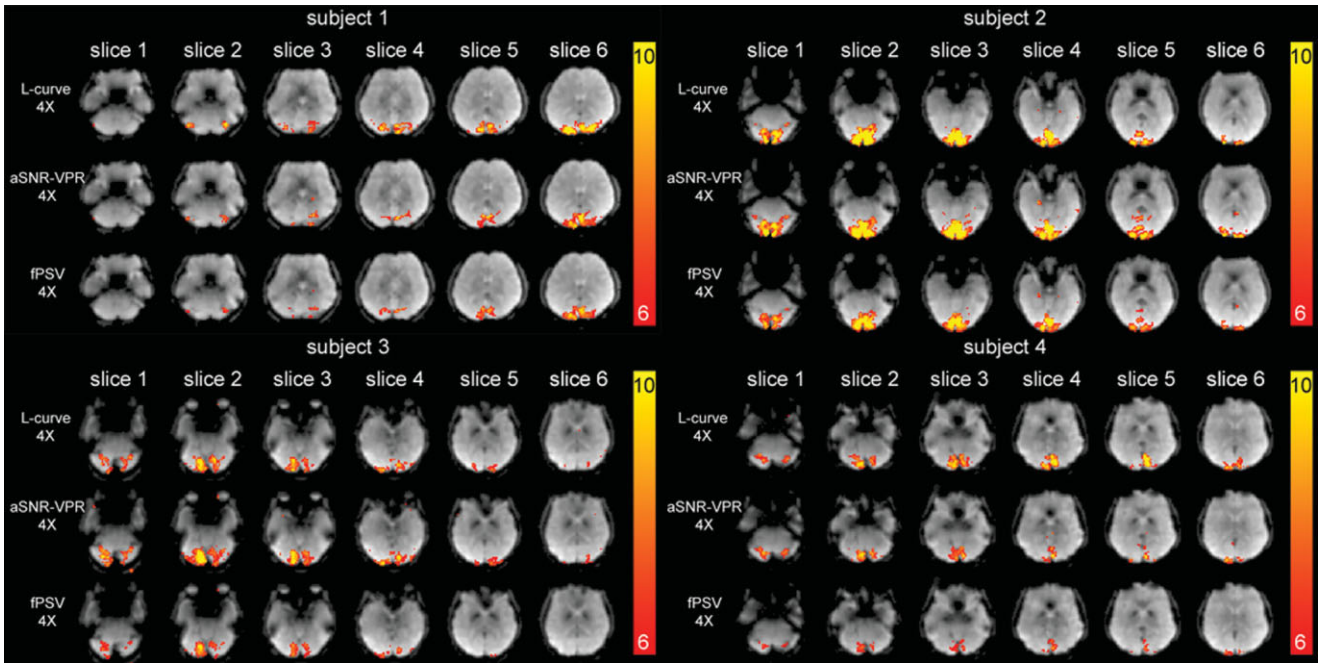

FIG. 8. The *t*-statistics maps of visual fMRI data in 4-fold SENSE accelerations with L-curve regularization, aSNR-VPR, and fPSV regularization.

model error term, which depends on the measurements of accelerated MRI data and estimated coil sensitivity maps in the context of parallel MRI. Thus, to quantitatively evaluate L-curve's performance, we used Monte Carlo simulations. Monte Carlo simulation is a justified method to evaluate nonanalytical systems utilizing the available modern computation technology (16), and it has been used in different disciplines of neuroimaging (17–24) and our previous study about applying the L-curve regularization in fMRI using parallel MRI acquisitions (8).

Given a fixed noise level, we would expect that the regularization parameter would be roughly invariant among repetitive measurements. Nevertheless, we observed that L-curve regularization provided a variable regularization parameter, possibly attributable to the ill-defined "elbow" region in an L-curve during regularization parameter estimation. Such difficulty is even more serious when the data have lower SNR. Qualitatively, data with low SNR will likely introduce a nonsmooth L-curve because of great variability in both the data and prior errors. Thus, the "elbow" region of an L-curve cannot be clearly defined. It has been reported that if the solution is "rough," i.e., that its Fourier coefficients decay at a rate slower than or equal to the singular values of the operator, the L-curve may fail to converge (27). However, a pure theoretical and mathematical analysis on the noise sensitivity of the L-curve method is beyond the scope of this study and will be further investigated in the future. From simulations, we found that the L-curve estimated regularization parameters with higher variability, particularly in cases of lower SNRs. In contrast to the L-curve method, VPR does not calculate measurement-dependent error metrics after noise whitening. Thus, we found regularization parameters estimated by VPR to be robust across iterative measurements in the same noise level. Using VPR for a robust estimation of the regularization parameter does not indicate that a constant regularization is optimal. This argument was validated by both structural and functional data: Fig. 3 shows the varying regularization parameters were estimated across frequency-encoded lines. And our fMRI results (Fig. 7) showed that VPR outperformed the reconstructions using the fPSV method. These results suggested that a regularization method adaptive to the quality of the acquired data, rather than a constant, can provide improved reconstructions. However, the instability and sensitivity of the L-curve method is a challenge, as indicated by Fig. 5. We proposed the VPR alternatives to mitigate this issue.

Compared to the L-curve approach, the VPR method presented in this work demonstrates computational efficiency at different image matrix sizes and SENSE acceleration rates. The accelerated regularization estimation process is derived from direct partitioning of the singular value spectrum. Unlike the L-curve approach, such partitioning does not involve an iterative search process to calculate the model error and prior error. The estimation process can therefore be accomplished at once. At the same image matrix size, we noticed that the improvement in computational efficiency was comparable at all SENSE acceleration rates. Given the estimated regularization parameter, the time to reconstruct a full-FOV SENSE image is identical with or without regularization due to the analytic solution written in our previous report (7). In fact, the estimated regularization parameter can be repeatedly applied to the dynamic measurement to keep constant bias toward the static prior.

The proposed VPR method has been adopted in other disciplines of regularization parameter estimation. For example, in general numerical analysis, some have suggested the inverse of SNR as an estimate of regularization parameter (16). Others have reported using SNR as an estimate of the regularization parameter for the source modeling of human electroencephalography (EEG) or magnetoencephalography (MEG) data (28). Like the L-curve approach, such regularization parameter estimation is fully automatic and is modified by the image quality of aliased pixels. Thus, unlike the fixed regularization approach reported by Sodickson (14), which uses 5% of the first singular value, VPR adapts to data quality and can dynamically estimate regularization parameter based on the noise level of the aliased pixel.

In this study we proposed using either aSNR or pSNR to estimate a regularization parameter. Even though stationary anatomical images showed better reconstruction using aSNR (higher regularization) than pSNR (lower regularization), caution should be taken in the following two aspects: First, an accurate prior for regularization is desired. Practically, if the prior does not match the model describing the generation of aliased images, for example, motion artifacts in dynamic scans after the acquisition of the prior image, highly regularized reconstruction may deteriorate the reconstruction quality. This is because the regularization biases toward a solution that does not fit the data. Second, in a dynamic scan looking for a high CNR, highly regularized results may decrease the contrast (contrast across time) more than suppress the noise level, and thus the overall CNR decreases. The overall effect of regularization on CNR needs more specific analysis depending on applications, because the competing suppressions in contrast and noise terms by regularization may either improve or degrade the final CNR. One scenario for using aSNR to partition the singular value spectrum is to reconstruct noisy parallel MRI acquisitions where the trade-off emphasizes suppression of noise level.

Employing the singular value decomposition of the encoding matrix to guide the search for optimal regularization has been reported by other groups as well (12,13). The proposed VPR method differs from those methods in its fully automatic calculation, while minimal heuristic intervention is required to define the abrupt change in singular value spectrum (13) or a user-defined constant to bound noise magnification from the RF coil array (12). A direct extension of the VPR method is to use the cutoff singular value determined by either pSNR or aSNR to implement the truncated Singular Value Decomposition (SVD), setting all singular values in the "noise" partition of the singular value spectrum to zero and thus increasing the stability of inversion of the encoding matrix.

In this study we performed regularized reconstruction for each individual frequency-encoded line. Mathematical analysis on the complexity of SVD computation indicates the advantage of using a line-by-line regularization over a scalar regularization for the whole image: The complexity of computing SVD on the encoding matrix, a necessary process to estimate a regularization parameter using either aSNR-VPR, pSNR-VPR, or L-curve method, is $O(n^3)$, where n denotes the

size of the data (29). Thus line-by-line regularization has computational complexity of $m*O(m^3)$ for a 2D image of m-by-m voxels. However, a scalar regularization for the whole image is of the complexity of $O(m^6)$. Following this complexity analysis, one may postulate that it may be even more computationally efficient if we separately analyze sets of voxels aliased to each observed voxels in the accelerated data in each individually frequency-encoded line, since the dimension of the aliasing voxel set (c-by-r for c-channel and r-fold acceleration) is even smaller than the dimension of line-by-line regularization ($m*c/r$-by-m for c-channel and r-fold acceleration). However, in such a case we will lose the resolution in the power spectrum of singular values owing to a very small dimension of the data. Consequently, we may likely miss the optimal regularization parameter estimation using the VPR algorithm, which select one singular values matched the estimated data SNR. In summary, we would argue that line-by-line regularization is both computationally efficient and provides sufficient resolution in the singular value power spectrum in regularization parameter estimation.

CONCLUSION

We have presented a computationally efficient and robust approach to estimate the regularization parameter for prior-regularized parallel MRI reconstructions. The proposed Variance Partitioning Regularization (VPR) algorithm is fully automatic and shows a significant reduction in computational time for different image matrix sizes and SENSE accelerations rates. We have also demonstrated that VPR provides more robust regularization parameter estimation than the L-curve method. VPR can be applied to either static structural or dynamic functional parallel MRI acquisitions for robust and computationally efficient image reconstructions with suppressed noise amplification and improved image quality.

ACKNOWLDGMENT

We thank Nichole Eusemann for preparation of the article.

REFERENCES

1. Sodickson DK, Manning WJ. Simultaneous acquisition of spatial harmonics (SMASH): fast imaging with radiofrequency coil arrays. Magn Reson Med 1997;38:591–603.
2. Pruessmann KP, Weiger M, Scheidegger MB, Boesiger P. SENSE: sensitivity encoding for fast MRI. Magn Reson Med 1999;42:952–962.
3. Kellman P, McVeigh ER. Ghost artifact cancellation using phased array processing. Magn Reson Med 2001;46:335–343.
4. de Zwart JA, van Gelderen P, Kellman P, Duyn JH. Reduction of gradient acoustic noise in MRI using SENSE-EPI. Neuroimage 2002;16:1151–1155.
5. de Zwart JA, Ledden PJ, Kellman P, van Gelderen P, Duyn JH. Design of a SENSE-optimized high-sensitivity MRI receive coil for brain imaging. Magn Reson Med 2002;47:1218–1227.
6. Tikhonov AN, Arsenin VI. Solutions of ill-posed problems. Washington, New York: Winston; distributed solely by Halsted Press; 1977. xiii, 258 p.
7. Lin FH, Kwong KK, Belliveau JW, Wald LL. Parallel imaging reconstruction using automatic regularization. Magn Reson Med 2004;51:559–567.
8. Lin FH, Huang TY, Chen NK, Wang FN, Stufflebeam SM, Belliveau JW, Wald LL, Kwong KK. Functional MRI using regularized parallel imaging acquisition. Magn Reson Med 2005;54:343–353.
9. Liang Z-P, Bammer R, Ji J, Pelc N, Glover G. Making better SENSE: wavelet de-noising, Tikhonov regularization, and total-least squares. International Society of Magnetic Resonance in Medicine; 2002, Honolulu, HI. p 2388.
10. Fuderer M, van den Brink J, Jurrissen M. SENSE reconstruction using feed forward regularization. International Society of Magnetic Resonance in Medicine; 2004, Kyoto, Japan. p 2130.
11. Tsao J, Pruessmann K, Boesiger P. Prior-information-enhanced dynamic imaging using single or multiple coils with k-t BLAST and k-t SENSE. International Society of Magnetic Resonance in Medicine; 2002, Honolulu, HI. p 2369.
12. Lin F-H, Chen Y-J, Belliveau JW, Wald LL. A wavelet-based approximation of surface coil sensitivity profiles fo correction of image intensity inhomogeneity and parallel imaging reconstruction. Hum Brain Mapp 2003;19:96–111.
13. Hoge WS, Brooks DH, Madore B, Kyriakos W. On the regularization of SENSE and SPACE-RIP in parallel MR imaging. International Society of Magnetic Resonance in Medicine; 2004, San Francisco, CA. p 241–244.
14. Sodickson DK. Tailored SMASH image reconstructions for robust in vivo parallel MR imaging. Magn Reson Med 2000;44:243–251.
15. Hansen PC. Rank-deficient and discrete ill-posed problems: numerical aspects of linear inversion. Philadelphia: SIAM; 1998. xvi, 247 p.
16. Press WH. Numerical recipes in C++: the art of scientific computing. Cambridge; New York: Cambridge University Press; 2002. xxviii, 1002 p.
17. Auranen T, Nummenmaa A, Hämäläinen MS, Jääskeläinen IP, Lampinen J, Vehtari A, Sams M. Bayesian analysis of the neuromagnetic inverse problem with l(p)-norm priors. Neuroimage 2005;26:870–884.
18. David O, Cosmelli D, Hasboun D, Garnero L. A multitrial analysis for revealing significant corticocortical networks in magnetoencephalography and electroencephalography. Neuroimage 2003;20:186–201.
19. Diedrichsen J, Shadmehr R. Detecting and adjusting for artifacts in fMRI time series data. Neuroimage 2005;27:624–634.
20. Lin FH, McIntosh AR, Agnew JA, Eden GF, Zeffiro TA, Belliveau JW. Multivariate analysis of neuronal interactions in the generalized partial least squares framework: simulations and empirical studies. Neuroimage 2003;20:625–642.
21. Liu AK, Belliveau JW, Dale AM. Spatiotemporal imaging of human brain activity using functional MRI constrained magnetoencephalography data: Monte Carlo simulations. Proc Natl Acad Sci U S A 1998;95:8945–8950.
22. Liu AK, Dale AM, Belliveau JW. Monte Carlo simulation studies of EEG and MEG localization accuracy. Hum Brain Mapp 2002;16:47–62.
23. Parker GJ, Alexander DC. Probabilistic Monte Carlo based mapping of cerebral connections utilising whole-brain crossing fibre information. Inf Process Med Imaging 2003;18:684–695.
24. Woolrich MW, Behrens TE, Beckmann CF, Jenkinson M, Smith SM. Multilevel linear modelling for FMRI group analysis using Bayesian inference. Neuroimage 2004;21:1732–1747.
25. Cox RW, Hyde JS. Software tools for analysis and visualization of fMRI data. NMR Biomed 1997;10:171–178.
26. Friston KJ, Holmes AP, Poline JB, Grasby PJ, Williams SC, Frackowiak RS, Turner R. Analysis of fMRI time-series revisited. Neuroimage 1995;2:45–53.
27. Vogel C. Non-convergence of the L-curve regularization parameter selection method. Inverse Probl 1996;12:535–547.
28. Hämäläinen M, Hari R, Ilmoniemi R, Knuutila J, Lounasmaa O. Magnetoencephalography-theory, instrumentation, and application to noninvasive studies of the working human brain. Rev Mod Phys 1993;65:413–497.
29. Golub GH, Van Loan CF. Matrix computations. Baltimore: Johns Hopkins University Press; 1996. xxvii, 694 p. p.